Probabilistic Estimates of Permissive Areas for Undiscovered Seafloor Massive Sulfide Deposits on an Arctic Mid-Ocean Ridge

Cyril Juliani, Steinar Løve Ellefmo
Norwegian University of Science and Technology (NTNU), Department of Geoscience and Petroleum, Sem Sælandsvei 1, 7491, Trondheim, Norway

Corresponding author: Cyril Juliani
Corresponding e-mails: cyril.juliani@ntnu.no, steinar.ellefmo@ntnu.no

Abstract

Norway explores its seabed mining potential including exploration studies on seafloor massive sulfides (SMS) at the outermost parts of its continental shelf, the Mohn's Ridge. Owing to the significant development potential and the general lack of knowledge of the SMS deposits, the evaluation of exploration targets and resource abundance are more than ever necessary. Given current exploration status, this study proposes to (1) develop a mineral prospectivity map (MPM) indicating favorable geologic environments for the occurrence of SMS deposits, and (2) estimate the number of yet-to-be found hydrothermal mineral deposits within volcanically active areas. The first part of this research focuses on the development of the MPM using a knowledge-driven approach. For this purpose, we apply the quantitative prediction framework characteristic analysis developed for terrestrial mining exploration. In this methodology, data must be captured and compiled into a relevant spatial data set that will be transformed, combined and weighted for prediction modeling. The data consist of morpho-structures and terrain attributes obtained from an interpreted bathymetric map. A multivariate analysis on the integrated data signature allow to calculate favorability values that will be projected on an exploratory grid. Each grid cell is given a likelihood of mineralization to indicate where SMS deposits might be located.

The second part of the paper estimates probabilistically how many SMS deposits remain to be found within neo-volcanic zones. These volcanic areas are geologically favorable to the occurrence of SMS deposits (permissive tracts) and provide the spatial basis for the probabilistic calculations. Estimates and associated confidence limits (10^{th} and 90^{th} percentiles) on the number of undiscovered deposits are

calculated using regression equations. The resulting probability distribution function presents an expected amount of 11 SMS occurrences undiscovered.

Keywords

mineral resource assessment; mid-ocean ridge; multivariate analysis; seafloor massive sulfide; GIS; exploration targeting

INTRODUCTION

Interests have been growing over the last decades in exploitable deep seabed mineral resources. Recent exploration activities have been extended to global tectonic zones in oceans, including the mid-ocean ridges (MORs) (Hannington et al., 2010). While researches are not only limited to territorial waters, industrial countries seek to investigate new resource minerals in more remote locations. In particular, seafloor massive sulfides (SMS) draw great attention due to their abundant commodities (e.g. Cu, Zn, Au and Ag). Despite the limited knowledge about SMS occurrences, governmental concerns for deep-sea mining led to significant needs in further investigations of valuable resource potential in unexplored regions of the ocean floor. In this context, the Norwegian Research Council has funded a project to investigate exploitation technologies relevant to potential deposits off the country's coast along a large part of the Arctic Mid-Ocean Ridges (AMOR) located inside the Norwegian jurisdiction. Specifically, the Mohn's Ridge has become an important subject of investigation where a few identified SMS deposits occur in various localities (Pedersen et al., 2010). Past investigations of the ridge indicated major characteristics genetically essential for seafloor mineralization (e.g. Dauteuil and Brun, 1996; Bruvoll et al., 2009), and confirmed the inference that there exist significant unexplored prospective areas, and thus a mining potential to be evaluated.

Accurate positioning and deduction of the number of undiscovered seafloor sulfides is very challenging since general exploration guidance often relies on extremely poor amount of data about SMS. Nevertheless, recent studies attempted to delineate and assess quantitatively SMS deposits along MORs (e.g. Hannington et al. 2011; Singer, 2014), and notably along a broad portion of the AMOR (Ellefmo and Sinding-Larsen, 2017). These estimates are commonly considered for different components among which the location and the number of mineral deposits that are integral

parts of a conceptual framework, the three-part form of mineral resource assessment (Singer, 1993; Singer and Menzie, 2010). This framework has been until now essentially applied for land-based studies (e.g. Singer and Menzie, 2010; Stensgaard et al., 2009; Eilu et al., 2015) and its application to unexplored offshore areas shall answer probabilistically the questions of "where" and "how many" mineral deposits are yet to be found in areas where limited geological and mineral occurrence data are available.

The outcome of estimating undiscovered occurrences is commonly expressed in terms of degrees of favorability within delineated prospective regions, i.e. the permissive tracts, in which geological criteria favor mineral deposits to occur (Singer, 1993). A technical way of achieving it is a proper management and compilation of targeted geological features extracted from data using a geographic information system (GIS). The power of combining data on a GIS-based environment offers efficient multivariate analysis for predictive mapping.

In an attempt to estimate where and how many SMS deposits may be found along the Mohn's Ridge, this paper will aim at developing and demonstrating how to produce a geologically-constrained predictive map of mineral potential, and ultimately evaluate probabilistically the number of undiscovered mineral deposits by regressive methods. For these purposes, identified geologic features are extracted from bathymetric data and then analyzed for subsequent evaluations of prospective areas and permissive tracts.

1. STUDY AREA AND DATASET

1.1. Study area

The Mohn's Ridge is an ultra-slow spreading center (<20 $mm.a^{-1}$) situated within the Norwegian-Greenland Sea that started opening approximately 55 Ma ago during the extension of the Mid-Atlantic Ridge (MAR) (Torsvik et al., 2001; Fig.1). It extends WSW-ENE for about 550 km from its southernmost part, delimited by the Jan Mayen Fracture Zone (JMFZ), to its northern junction with the Knipovich Ridge. The ridge presently spreads at a rate of about 15 mm/yr (Vogt, 1986) with an oblique relative displacement between 30° and 45° (Fournier and Petit, 2007). Toward its center, the mean crustal thickness is of about 4.0 ± 0.5 km (Klingelhöfer, 2000), a thickness considered lower than average

for normal crust formed along the MAR, but typical at ultra-slow spreading ridges generally showing thinner and variable crustal thicknesses (Chen, 1992).

Apart from the anomalous segment adjacent to the Jan Mayen, water depths at the axial valley of the Mohn's Ridge range in average from 2.5 to 3.1 km and decrease progressively toward the southwest due to its proximity to the Jan Mayen hot-spot (Neumann and Schilling, 1984; Schilling et al., 1999). A characteristic aspect of the rift bathymetry is the strong asymmetrical configuration of the flanks delimiting globally higher summits on the north-western sides. Moreover, the axial valley and the bounding flanks are marked by series of en-échelon ridges interconnected by non-transform offsets (NTOs) that somewhat describe variations in the ridge obliquity. This segmentation pattern occurs with intermittent volcanism characterized by basement highs elongated at the scale of approximately 20-30 km and oriented perpendicularly to the spreading direction. Previous studies distinguished these ridge segments to be volcanic edifices (Géli et al., 1994) while some involved tectonic origins solely with trans-tensional bounding-faults (Dauteuil and Brun, 1993; Dauteuil and Brun, 1996).

Bathymetric data of the Mohn's Ridge have been collected by the Norwegian Petroleum Directorate (NPD) in collaboration with the Geological Institute of the Russian Academy of Sciences (GIN RAS). The data have been used to create a digital elevation map (DEM) that has been stored in a regular grid network (square grid) of 50m-cells resolution, using GIS-based software. The data cover most of the rift valley from the JMFZ to the bend with the Knipovich ridge (ca. 73°N, 8°E). Investigation of the multi-beam data shows that the width of the axial rift valley, i.e. the distance between the rift walls, ranges from 7 to 16 km. The axial valley often deviates at NTOs where deep basins (≥ 3-km depth) trend at ~30° from the ridge axis within a spacing range of 18 to 25 km. These basins usually lack recognizable structures or volcanic edifices, but are commonly bounded by large dextral E-W transverse faults possibly accommodating the depth variation of the brittle/ductile boundary (Dauteuil and Brun, 1996). NTOs have limited lateral structural expression, but their off-axis traces remain visible from alternating sets of continuous ridge-parallel terrains and from structures that trend slightly oblique to the spreading direction. The volcanic activity at these transitions are quite restricted, and importance of such zones for hydrothermal venting remains to be shown.

In the south-western part of the ridge, segments and NTOs are difficult to identify because of irregular and complex bathymetric patterns associated to abnormally abundant volcanic activity and curved tectonic structures. In this region, the melting anomaly can be associated with more shallow and smoothed terrains because of the southward Jan Mayen hot-spot interaction, whereas the curved structures respond with strike-slip displacements along the ridge walls (Dauteuil and Brun, 1996). In contrast, the northernmost Mohn-Knipovich bend consists of a magmatic-starved segment with more symmetric flanks expressing a rough topography at the higher western side compared to the sediment-covered eastern flank where only a few basement ridges are exposed. Along the overall ridge, the western flanks are on average 200-m higher than the opposite side, due to higher tectonic activity. Their edges may sometimes correspond to rotated and uplifted fault blocks forming downward curved ridge flanks that are usually attributed to low-angle detachment surfaces (Smith et al., 2008).

According to existing geological data, the general combination of volcanism and tectonic activity within the different segments of the Mohn's Ridge creates favorable conditions for hydrothermal systems to have heat and fluid circulation, which make it possible to form massive sulfide deposits. So far, interesting SMS occurrences have been found along the ridge, exemplified by the Loki's Castle vent field and Copper Hill (Pedersen et al., 2010) (Table 1).

2. METHODOLOGY

Because there exists a strong spatial and temporal correlation between hydrothermal manifestations and faults, deep magmatic activity, depth and basement properties, predicting potential locations for SMS deposits requires assimilating these factors. For convenient integration, analysis and processing of available geo-spatial information, the data are managed using a staged methodology:

1. Identification of prospective criteria associated to ore mineralization (morpho-structural analysis) and digitization of geological features
2. Creation of spatial evidence maps (logical transformation)
3. Combining of evidence maps into a regular squared grid in which cells determine different degrees of favorability for the occurrence of mineral deposits (favorability calculation)

4. Modeling of potential mineral exploration targets (probabilistic analysis)

This conceptual modelling uses a knowledge-driven approach from which the evidence maps are weighted and then combined to develop a prospectivity map.

2.1. Morpho-structural analysis

Investigations on present-day locations of SMS deposits reveal several consistent morpho-structures associated to the generation of vent fields. To develop reliable predictive analysis for prospective areas, we produced from the DEM detailed morpho-structural maps (Fig.2 and Fig.3). The analytical process involved the use of basic terrain parameters (slope, curvature, and slope direction or aspect) as well as several bathymetry images obtained by numerical processing of multi-beam data. This includes simulated shaded relief for morphological characterization at diverse lighting directions and principal component analysis (PCA) of the bathymetry that distinctly outlines various directional trends (or lineaments) in the multi-beam data. PCA is a multivariate statistical technique for dimension-reduction of dataset into smaller-dimensional subspace (Davis, 2002). It is commonly used to reveal simpler patterns within a set of variables so that interrelationships within the data can be characterized and mapped. In combination with contour maps, the PCA method is best suited for detecting linear structures, and can be correlated with both the slope steepness and the aspect to indicate components of fault trends (azimuth, length, and shape).

To better support direct visual interpretation, we also performed a semi-automatic interpretation of the bathymetry using various image processing techniques: (1) the edge-based filter Canny (Canny, 1986) for the recognition of potential fault traces, and (2) the Hough Transform (Duda and Hart, 1972) to detect a variety of arbitrary shapes related to escarpments and volcanic manifestations. From these, we collected an extensive dataset of geoscientific information to identify the exploration targets.

2.1.1. Neo-Volcanic Zones

High-temperature hydrothermal systems are commonly related to neo-volcanic zones (e.g. Fouquet et al., 1993; Murton et al., 1994; Münch et al., 2000; Webber et al., 2015). These areas have both, volcanic and tectonic activities that are a prerequisite to develop a heat source and pathways for fluids convection. Along the Mohn's Ridge, the volcanic areas identified can be relatively narrow and sparse, or expressed as linear topographic highs oriented normal to the spreading direction are formed. The later are known as axial volcanic ridges (AVRs), i.e. elongated domed edifices built of

agglomerations of volcanic hummocks (Smith and Cann, 1990; Yeo et al., 2012) for which life cycle can be comprised between magmatic and amagmatic phases during the ridge evolution. The main edifice can break apart and possibly be rifted off the axis when it is subject to tectonic activity (Parson et al., 1993; Mendel et al., 2003; Peirce and Sinha, 2008).

Correspondingly, the individual hummocks have variable surficial expressions and spatial extents that range within 2-9 km in width and 15-29 km in length inside the rift valley. They can present distinct tectonic structures interpreted by Dauteuil and Brun (1996) as horsts, grabens, titled blocks and domes, revealing the close relationship between constructional volcanism and tectonic deformation within the axial valley. Alternatively, other southward ridge segments often display abundant large volcanoes and smooth lava flows distributed along-axis, probably indicating higher effusion rates during phases of high magmatic flux (Clague et al., 2000). These variabilities apply to differing tectonic phases and eruption styles associated with each AVR that may either extend from the center of the valley to the base of the bounding axial valley walls, or remain surrounded by areas of flatter and deeper seafloor. These observations among the AVRs reveal that effective volcanism dominates at some, while at others there is little evidence of recent magmatism and tectonism dominates.

Adjacent to the AVRs, the ridge walls commonly show series of parallel ridges with similar morphology and typical hummocky terrain indicating old pieces of AVRs transported off-axis. The major bounding faults of the median valley sometimes tend not to fully disaggregate relict AVRs that, in this case, can be preserved more or less intact and, on the same way, possibly retain old extinct basalt-hosted vent fields.

2.1.2.Faults

Faults are strong indicators for localized hydrothermal venting because they could potentially develop pathways for fluid convection, allowing hydrothermal circulation and focused outflows (McCaig et al., 2007). Within the inner valley of the Mohn's Ridge, observable faults concentrate essentially at the AVRs affected by repeated rifting that create fractures and repeated faulted seafloors ripped off from the ridge axis. In this context, hydrothermal systems may develop either from across-axis trending grabens, tilted blocks running off-axis or tectonized volcanic domes. On the other hand, the transitional deep basins show little sign of faulting; they have a flat surface, sometimes with undulations probably attributed to older topographic breaks subsequently covered by lava flows and/or sediments.

Off-axis, the westernmost bounding faults generally have large offsets providing pathways for deep, along-ridge hydrothermal circulation. Some flank complexes with very large elevated massif may supposedly develop long-lived detachment faults sustaining more distant hydrothermal circulations across axis (e.g., Petersen et al., 2009; McCaig et al., 2007).

Within the axial valley and at the ridge walls, two types of linear structures can be recognized: the ridge-parallel faults delimiting minor and well-developed scarps, and oblique tectonic dislocations propagating linearly. The latter is identified when topographic features offset laterally, or sometimes, when oblique volcano alignments occur during tectonic disruptions. Due to the data resolution, in most cases, we cannot distinguish these linear traces as either fault zones, single fault planes or fractures. For this study, the term fault is preferred as detectable features regularly affect the topography at kilometer scale. In this context, the distribution of averaged fault directions shows two populations: near-parallel or oblique to the ridge trend (ca. N045°), and oblique to the strike direction of the neo-volcanic ridges (ca. N315°). When compared, axis-parallel faults have orientations globally less variable (with a standard deviation of 17.27°) than those from the oblique faults (41.37°) indicating that these orientations depend considerably on the angle between the rift zone (N055-070°) and the extension axis (N110-120°; Dauteuil and Brun, 1996). With two deviating trends, faults commonly intersect at places where they accommodate irregular seafloor deformation, indicating potential loci of permeability to focus hydrothermal fluids. These intersections at cross-cutting faulted features are essentially localized either between segments, where oblique strike-slip fault motions are expected (Dauteuil and Brun, 1996), or within well-developed rift valleys splitting-off AVRs.

2.1.3. Volcanoes

Active and inactive volcanoes represent obvious indicators for areas assumed to host or have hosted underground heat sources. Using images processing techniques, various types of volcanic structures are recognized and located on the bathymetry. In particular, the most widely distributed flat-topped volcanoes are well-developed along the axial valley of the Mohn's Ridge, but are not uniformly distributed. Among the 557 largest volcanoes observed (>0.15 km2, including crater-type or flat-topped type), most of them are located either on the flanks of the axial highs and toward their bottom depression, or at the segment-ends (i.e. between the axial basins and the elevated axial highs). However,

a few cover the basins, and old relict volcanoes are preserved at the ridge walls. The southern part of the ridge, in contrast, shows an unusual abundance of volcanic structures associated with the various morpho-structural settings at the ridge valley floor, and at its easternmost flank. In general, the volcanic structures evolve such that minor volcanic manifestations (< 0.06 km2) develop successively to form overlapping hummocky-like seafloor. Alternatively, faults may cut them in pieces, resulting into relict volcanic evidences.

2.2. Knowledge-driven modeling of SMS deposits

The analytical study of the DEM can be generalized to a certain number of raster-transformed evidence maps. Correspondingly, 11 quantified characteristics (variables) of 8 prospectivity criteria deemed to be significant for the occurrence of SMS deposits, have been established (Table 2). They consist of morpho-structural features for which their spatial influence is expressed quantitatively (e.g. distance and density). The variables are selected based on several consistent observations related to vent deposits located at volcanic ridges along the MAR, and on the analysis of the Loki's Castle vent field area (Table 1) that is considered here as a reference for the SMS prospective model.

For the SMS deposits considered here, i.e. either from active or inactive venting sites, prospective geological environments are characterized by the presence of, or the proximity to geological features that may indicate potential mineralizations. In mineral potential mapping, these environments are only indicative criteria because SMS deposits are not necessary present in every area geologically favorable.

2.2.1. AVRs

Seafloor hydrothermal activity occurs in a wide variety of geological settings along slow-spreading MORs (Fouquet et al., 2010), raising up more attention toward geological interpretations. This complicates prediction models that can be more problematic to interpret if wrong assumptions are involved about the investigated seafloors and/or if no appropriate deposit reference is available. Therefore, general simplifications are made to integrate exclusively the neo-volcanic zones relative to the axial valley of the Mohn's Ridge, leaving other non-considered ridge components uncertain as prospective areas. These volcanic zones are prevalent targeting sites considering the significant discoveries made on volcanic ridges (Hannington et al., 2010). They usually constitute environments with small-scale faulting

associated with dike emplacement and high geothermal gradients (e.g., Germanovich et al., 2000; Carbotte et al., 2006) that both offer significant possibilities for hydrothermal convections throughout the renewed crust.

2.2.2. AVR proximity and ridge distance

AVRs are strong indicators for underlying heat source whose heat transfer plays a major role in hydrothermal circulations. Distances from the centerline of the ridge valley are in this study calculated so that a given proximity to the ridge-centered volcanic zones indicates certain degrees of favorability for hydrothermal occurrences (Table 3). Attributing geological importance to proximal indicators is not obvious since it requires a much better understanding of the underlying geological processes controlling hydrothermal systems and associated ore mineralization. Alternatively, quantitative and qualitative measures help estimating empirically the distance-to-mineralization relationship if we consider, for example, similar information about the location of known active high-temperature vent systems. Presently, a few data about the estimated distances of basalt-hosted vent deposits from ridge-axes have been reported along the ridge valley of slow-spreading ridges (e.g. TAG (Rona, 1993); Moytirra (Wheeler et al., 2013); 14°S (Li et al., 2014); and Beebe (Webber et al., 2015) vent fields). Their estimated average distance reaches about 3 km, while tectonic-associated deposits in active high-temperature systems can reach the seafloor 7 to 8 km off-axis (e.g. Ashadze, Logachev, Semyenov, Logachev and Nibelungen vent fields; Fouquet et al., 2010). Because the along-axis thermal regime of ridge segments may change in space and time (Shaw and Lin, 1993; 1996), the state of oceanic accretion is variable from segment to segment (Parson et al., 1993). Therefore, the proximal indicators used in this study should be considered as statistical estimates rather than realistic measures for heat source influence.

On the other hand, distant hydrothermal systems (> 3 km from axis) observed on the MAR are generally associated to later stage detachment systems that often control episodic mafic intrusions occurring as heat sources either near the ridge axis or emplaced into the ultramafics of an oceanic core complex (OCC) (Pertsev et al., 2012). Alternatively, elevated heat fluxes may be a transient heat from the lithospheric mantle of the nearby ridge sections. This variability in heat source mined from cooling magmatic bodies cannot be evaluated for exploration purpose as no structural evidences indicate it. Therefore, the predictive distance interval of 3 to 8 km is defined as unevaluated in the prospectivity map.

2.2.3.Fault proximity

As fault traces were digitized from a 1:100,000 scale bathymetric map, uncertainties exist about their precise position and the potential faults offset from their actual locations. Likewise, it is unsure where SMS deposits are situated relative to the faults as dispersal surrounding fractures may develop locally and provide in-situ new pathways for migrating fluids. On the basis of measured fault scarp lengths (mostly < 500-m horizontal distance within AVRs) and in-situ position of the Loki's Castle occurrence to a major fault (within 500-m distance), this uncertainty is handled by using a 500-m buffer distance around the faults to account for potentially mineralized zones. Buffer intervals with fixed widths cannot guaranty proximal mineral deposition but are rather reasonable approximations for effective research areas.

2.2.4. Proximity to fault intersections

When interacting, faults may create and maintain permeability by concentrating stresses and fracturing in the crust (Curewitz and Karson, 1997). This leads to zones of greater rock permeability, which can favor hydrothermal fluid circulation over extended areas. High-temperature outflows have previously been considered in zones controlled by intersection of the along-axis and obliquely trending faults (e.g. TAG (Karson and Rona, 1990), Broken Spur (Murton et al., 1994), Ashadze-1 and Krasnov (Cherkashov et al., 2008) and Moytirra (Wheeler et al., 2013) vent deposits). Although these associations of cross-cutting faults and vent sites look quite promising for prospectivity, specifying the extent they played in seafloor mineralization remains uncertain. Intersection indicators are thus characterized quantitatively at buffered distances (500 m; Table 3) that may cover areas with a chance to include undiscovered deposits.

2.2.5. Volcano proximity

Past discoveries showed that vent fields may develop on well-developed volcanic edifices, such as sites involving either flat-topped volcanoes (Squid Forest vent field; Pedersen et al., 2010), or a rifted central volcano (Lucky Strike vent field; Langmuir et al., 1997), or associated to young volcanism on flat volcanic reliefs (Turtle Pits and Confortless vent fields; Haase et al., 2007). Therefore, location of large flat-topped volcanoes, volcanic mounds and crater-type volcanoes represent additional exploration evidence to locate potential resource prospects. They are characterized at a certain distance buffer (Table 3) to account for neighboring major structures and possible small-scale fracturing evidence not recognized in our data.

2.2.6. Densities

A probability density function of geological features (i.e. faults, volcanoes and fault intersects) was calculated using kernel density estimation. The degree of spatial correlation between variables is dependent on the distance between features, and thus the distance of search to calculate the density (kernel bandwidth). To obtain the bandwidth, we performed a proximity search around geological features. The resulting estimates give the average closest distances between features (Table 4) that will be used as bandwidths for the density estimates. Density variations of geological features provide indirect information about the reflectance characteristics of particular areas. For example, a localized spot of high-density fault may reflect areas with enhanced rock permeability, implying possible continuations of favorable geologic environments for mineral deposition at more regional scale. On the other hand, the density of geological data is insufficient to certify detailed interpretations at the deposit scale. For this reason, it better corresponds to a predictive variable for identifying favorable environments of mineralization.

2.2.7. Depth

Water depth is another factor that significantly affects the precision of prediction. Copper-enriched SMS deposits are typically associated with high-temperature (> 300°C) venting systems, while low temperature vents usually show higher zinc content (Large, 1992). Similarly, SMS distribution over different depth intervals reveals variable metal content; e.g. deposits occurring at 1,000-m water depth often display Cu-rich deposits, while higher Zn content is expected at shallower environments (Monecke et al., 2014). These observations have often been attributed to boiling hydrothermal systems in which hydrothermal fluids affected by phase separation may involve loss of components such as H_2S which is essential for sulfide mineral deposition on the seafloor (Drummond and Ohmoto, 1985). Boiling commonly occurs with reduced hydrostatic pressure (Monecke et al., 2014), and accordingly, water depth eventually restricts high-temperature venting in shallower environments. This temperature-to-depth control over sulfide mineralization has major effects in the metal content of sulfide precipitates on the seafloor. A majority of known hydrothermal vents on worldwide MORs occurs at depths (> 1,500 m) that usually involve boiling effects in hydrothermal systems (Beaulieu et al., 2013). On the other hand, further estimates also constrained the minimum depth (852 m) at which the maximum temperature of 300°C is reduced (Monecke et al., 2014).

2.2.8. Slope

Very few vent deposits have been reported with steep slopes environments. For example, the basaltic seafloor of the Krasnov area (lat. 16°38’N) has an average slope of 32° (Cannat et al., 2013). In this setting, estimated critical slope

for non-cohesive basaltic surface is at least 26°. Above these angles, numerous rockslides and gravitational collapses may affect pre-existing deposits during in-situ tectonic displacements and erosion of the axial valley relief. As the relations between surface instabilities and natural flows, volcanism and hydrothermal activity are unclear yet, seabed sloping of more than 32° is not evaluated (Table 3).

2.2.9. Scarps

In rough terrains, active hydrothermal systems are frequently associated to distinctive escarpments (e.g Kelley et al., 2005; Wheeler et al., 2013; Fouquet et al., 2010). Generally, these represent expected locations of active venting, because of the genetic nature of faults believed to be the dominant control on upper-crustal permeability that localizes venting in a given area. Likewise, scarps of tectonic or volcanic origin usually show prevalent exposure of more complex structures firstly identified for potential exploration targets because vent systems are often nestled against areas that present great deals of heat supply and/or rock failure.

2.3. Ternary transformation

In mineral exploration, the analysis of geological variables requires quantitative procedures by which pertinent exploration data are analyzed, integrated and quantified. McCammon et al. (1983) developed a multivariate technique called the characteristic analysis (CA) that allows development of decision-making models for mineral exploration. It is achieved through the transformation and combination of geological data. By associating the data, it describes quantitatively degrees of importance (weight) of each geological variable using probabilistic calculation.

In this study, the CA has been implemented in a GIS-based environment to process evidence maps. The pre-processing step involved an integration of variable attributes into regular grid of cells to generate ternary maps. Ternary representation of data allows classification of areas as being either favorable or unfavorable for mineralization with respect to chosen variables (McCammon, 1983). It also provides standardization of quantified or non-quantified data for subsequent analysis. In this context, the ternary values have been attributed to the different evaluation criteria for the occurrence of SMS deposits in the table 3. Correspondingly, the ternary coding expresses either favorable or unfavorable conditions (+1 or -1 respectively) or situations where the effect of an attribute on predictions is considered

unknown or unevaluated (0). This way of re-evaluating raster evidence maps permits control on the proximity and the density values that influence the relative importance of cells depending where they are located.

Final ternary maps result in raster grids of 100-meters squared cells characterized by the predictive classification values. Because sulfide deposits may hold different mineralized extents, and thus show different physical sizes, the cell size might present problems to estimate a certain number of deposits in a cell with respect to its calculated favorability. For this reason, cell-based probabilities of discovering one or no deposit shall not be considered as general guidance to estimate a number of undiscovered deposits.

2.4. Favorability calculation

Spatial association between geospatial data is critical in mineral exploration as targets can be identified in areas where some anomalies coincide. Multivariate analysis methods can be applied to identify these associations because it provides clear mathematical expressions of the relationship between variables (McCammon, 1983). Among existing conventional statistical models, PCA can compute estimates for the occurrence of mineral deposits (or favorability values) on the basis of linear combination of the ternary transformed data. PCA was previously used for bathymetric studies (cf section 2.1). It is also used here to calculate the weight coefficients of the geological variables. This mathematical approach is demonstrated in the appendix A.

2.5. Deposit modeling

Predictive modeling of mineral exploration targets in the characteristic analysis uses established deposit models from which observations are taken in and around known ore deposits (McCammon et al., 1983). Technically, a deposit model consists of a selected set of cells (control cells) characterizing a specific setting for mineralized areas within a given region. The control cells can be compared with other cells such that any matching may reveal potential mineral targets if compared characteristics are close enough with those of the known deposit type. As stated by McCammon et al. (1983), such model (M1) cannot be based solely on cells that contain known accumulations because it would be too restrictive in its application in other areas. Instead, other regional cells similar to cells in the model M1 shall be integrated, but these might not contain any SMS deposit. By doing so, the model (M2) risks to be overgeneralized

because other cells with unrelated variables are included. One way to avoid this is to refine the generalized model M2 by identifying the unrelated cells. This can be done by re-calculating the characteristic weights of the variables for the cells of M2, and then selecting the cells with the highest significance for being related to SMS deposits. To calculate the significance of these cells, we follow a generalized procedure testing whether the degree of match between cells of M1 and M2 (that includes M1) is purely due to chance or whether there exists a significant relationship between them (cf. McCammon et al., 1983 and appendix B). This approach gives a final refined general model (M3) where unrelated cells have been removed. For this study, the initial model M1 was expanded to 69 cells and then refined to a model of 22 cells for which corresponding weight have been calculated for the 11 variables (Table 5). While M1 strictly corresponds to an area with SMS deposits, M3 represents the geologic setting associated to seafloor mineralization that can be used as an exploration model to be compared with other areas. Areas sharing same characteristics of M3 can be regarded as potentially hosting mineral deposits.

2.5.1. Mineral targets

An analytical modeling of SMS deposit targets is achieved by re-calculating the favorability map weighted by the weight values of M3 (Table 5). The map is then analyzed spatially by comparison with the model on the basis of (1) the characteristics observed, and (2) the favorability scores obtained for the re-calculated map. The control cells describing the Loki's Castle vent field area consist of at least the 9 most important characteristics outlined from the calculated weight (i.e. 0.321 in table 5), and the sum of their favorability scores gives 68.41. These 2 significant values indicate that a mineral target is estimated from a strong spatial relationship between the morpho-structures and the bathymetric attributes. Significant relationships have obviously increased favorability scores when more characteristic criteria are correlated. Hence, the number of characteristics and the sum of favorability scores represent two predictive values that can be used as minimum criteria for target investigations. The targets are obtained by comparing the deposit model with other areas in the re-calculated favorability map. Using an automated analytical process on the GIS-based software, the favorability map is analyzed to identify potential exploration targets that verify these conditions. If they do, one mineral target is plotted at a position where any findings could be made within 300 m. The predictive distance is determined from the deposit model itself to cover a favorable geological environment.

3. Estimating numbers of undiscovered mineral deposits

While exploration surveys have made significant progresses in the last decades, low amount of reliable data make it difficult to estimate how many SMS deposits remain to be found. However, extensive knowledge of land-based volcanogenic massive sulfide (VMS) deposits allowed the development of effective prediction tools adaptable in the evaluation of SMS deposits. In quantitative resource assessment, estimating numbers of undiscovered deposits can be established probabilistically from calculating the density of deposits (deposit / km2) in areas where the geology permits the existence of one or more types of mineral deposits, i.e. the permissive tracts (Singer 1993). Singer et al. (2001), Mosier et al. (2007) and Singer (2008) summarized this idea by estimating densities for different types of volcanogenic massive sulfide (VMS) deposits through regression equations based on the comparison between the distribution of deposit densities and well-explored permissive control tracts. Singer and Kouda (2011) subsequently generalized these approaches through the analysis of several deposit types from worldwide explored permissive tracts and found strong relationships between deposit size, area permissive, and deposit density. They estimated deposit densities using a regression model based on permissive control areas and deposit tonnages and concluded that the size of the permissive tracts can be used directly to estimate the number of deposits at different prediction levels (i.e. 10th, 50th and 90th percentiles, cf. Appendix C).

In comparison to the VMS-based regressive model of Mosier et al. (2007), the predictive concept from Singer and Kouda (2011) is dependent on the median deposit size estimated for the deposit type considered. This concept is preferred in this research because (1) the density and size of seabed ore deposits are generally a function of spreading rate (Hannington et al., 2011), a peculiarity not treated by Mosier et al. (2007) among the VMS deposits studied, and (2) no well-explored (drilled) known deposits can serve as basis to estimate the number of undiscovered deposits (as required by the predictive concept from Singer and Menzie, 2010) and thus, we assume that the general model is best representative of the deposits yet to be discovered in the tract.

3.1. Permissive tracts

Permissive tracts represent extended frontiers of terrains for which geologic environments permit a deposit type to form (Singer, 1993). Beyond those frontiers, the probability of occurrence for new findings is negligible for the deposit type considered. Inside the tracts, the deposit targets previously generated restrict mineral exploration into in-situ areas similar to a predefined model and are therefore only intended to be used for prospecting purposes. Aligned to the

targeting studies, we also consider estimating numbers of undiscovered deposits with similar setting to the Loki's Castle area. Hence, the tracts shall stay consistent with the prospective criteria and the model proposed (Table 2 and 3) by including the morpho-structural units and seafloor properties. For consistency and simplification, the delineation of the tract boundaries is traced following the recognizable extents of neo-volcanic zones (i.e., the rough unsedimented basaltic terrain, including the AVRs). As the ridge valley floor presents segmentation patterns and variable terrains, this delineation preserves the general elevated topography by taking away the flattened terrain not affected by disrupting structures, i.e. those usually considered as hosting lava lakes or sediment covers, and lacking of fault signatures. As a result, no probabilistic inferences are established on the potential deposits at older crusts.

This approach would, in normal case, disregards the standard rule implying that the occurrence of undiscovered deposits outside the tracts is probabilistically negligible, but for this study, the estimates are established for deposits that mimic the geological setting of the reference model. Hence, predicted numbers of deposits are considered associated with recent and active (or inactive) hydrothermal systems in volcano-tectonic ridges. It is noteworthy that more extensive permissive areas in these circumstances could overgeneralize the tracts by taking non-permissive rock units, and thus, biasing the probabilities resulting from them. In this context, future cautions should be taken while interpreting the associated estimates because permissive tracts are dependent on the deposit type sought.

In total, 34 tracts were obtained for about 2922.53 km2 of permissive areas accounting for approximately 55% of the overall ridge valley floor (Table 6). Although these tracts represent essentially sections of neo-volcanic zones, undiscovered SMS deposits are more likely to be discovered first in these zones because knowing the significant occurrences of vent fields hosted in these settings along slow- and ultra-slow spreading ridges (Fouquet et al., 2010; Hannington et al., 2010), exploration would likely focus on these volcanically robust areas.

3.2. Prerequisites for estimations

The relevance of using the regression model resides in its suitability to be used for any deposit type, in particular deposits hosted in mafic assemblages for which the median size is assumed to be known. At present-day, SMS deposits lack of reliable occurrence information for meaningful assessments of both their size and spatial distribution. As VMS deposits and SMS deposits have analogous genetic and spatial relation with contemporaneous volcanism (Hannington

et al., 2005), ophiolitic VMS deposits hosted in basaltic volcanic rocks represent valuable models in the quantitative assessment. Correspondingly, the calculated estimates for this study consider a median deposit size (0.9 Mt; Mosier et al., 2007; Singer, 2008) taken from the available tonnage distribution of Cyprus massive sulfide deposits hosted in the basaltic extrusives of the Troodos ophiolite (Mosier et al., 2007).

Although some other uncertainties about the geologic setting of the Troodos ophiolite exist, general studies tend to describe the Cyprus tectonic setting as a portion of oceanic crust and mantle generated during a rifting. The general consensus implies a formation by seafloor spreading at a supra-subduction or in a subduction initiation setting (Rautenschlein et al., 1985; Pearce and Robinson, 2010) while some involved a single slow-spreading axis (Moores and Vine, 1971; Abelson et al., 2001). Previous studies also described the Cyprus sulfide deposits as presenting strong similarities in morphology, mineralogy and ore genesis derived from processes similar to those presently observable in active vent fields at the MAR (Hannington et al., 1998). In addition, the Troodos ophiolite presents important advantages for the estimates here because, in comparison to most of the few ophiolites known to host Cyprus-type VMS deposits (i.e., at least 25; Galley and Koski, 1999), (1) it preserves records of axial hydrothermal activities in the upper crustal section throughout the basaltic section (Cann and Gillis, 2004), (2) information about spreading rate is available (Moores and Vine, 1971; Abelson et al., 2001), (3) it avoided significant syn-tectonic modification processes (e.g. deformation and metamorphism; Cann and Gillis, 2004) keeping exploitable massive sulfide evidences, and (3) the exposed VMS deposits are already extensively studied in the extrusive rocks (e.g., Adamides, 2010a,b). This gives insights on the spatial correlation between deposits.

Estimating deposit densities by translating permissive areas from an ancient MOR system with the slow-spreading MAR requires some cautions though, since the Troodos ophiolite could still possibly contain buried deposits not yet discovered (Jowitt, et al., 2005), and erosional processes may have contributed in sulfides loss before the ophiolite reached its final position on land. However, a major consideration for density evaluation reside in that the fossil deposits in Cyprus were formed in the same way as modern deposits of MORs, meaning that processes involved in the formation of these mineral deposits are still operating in typical way today.

4. RESULTS

4.1. Weight characteristics

The different characteristic weights of variables produced from the regionally calculated favorability are shown in the table 7. The coefficients of the first component do not show systematic changes and even the sign of the loadings stays unchanged. This is not unexpected since the ternary maps give all sampled geological features initially accounted to favor mineral deposition (weighted +1), a behavior that PC1 seems to express here. 10 of the 11 original variables are strongly correlated with the first principal component, suggesting that most of them are redundant and vary together. The degree of relevance for mineralization in an area will therefore depend on its number of attributes. Moreover, the correlation among the variables is mainly influenced by the seafloor properties, the distance to volcanic zones and the density of faults, outlining the significance of possible regions with enhanced rock permeability and heat production translating potential mineralization.

Most of the geological features have a high weight coefficient (≥ 0.187; Table 7), suggesting that they have a strong effect on the first principal component. However, slope (0.026) and depth (0.015) do not seem to play a significant role in explaining the variance of the analyzed combined data. The contrasting difference between these results derives from the regional analysis (within the ridge valley). Geological features that tend to be genetically related (e.g., faults, fault intersects, and volcanoes), locally occur close together at the escarped and/or rough volcanic terrains of AVRs. On the other hand, variables of lowest rank (slope and depth) have widespread occurrence across the ridge and have thus no particular relationships to the above-mentioned local features. Compared to the regionally calculated weights, the loadings from M3 show a slightly different trend by downgrading faults trace and intersections. A target mineral is therefore supported by most of the geological features present, while areas regionally favorable are dominantly represented by distance to volcanic structures, density of faults and seafloor expression.

4.2. Regional prospectivity mapping

The regional prospectivity map has been generated over 510 km along the Mohn's Ridge by summing the weights of the evidence maps (Fig.4). The various combinations of these maps result in the highest scores for the locations where

all the favorable geological characteristics are present. In contrast, the lowest scores are located where favorable conditions are scarce or absent (mainly distant areas from the ridge axis). The predictive cumulative weights range from 2.97 (Table 7) to a minimum of -2.54, prioritizing highly prospective areas essentially located on AVRs and close to ridge axis. In detail, favorable areas most likely have regionally abundant favorable morpho-structures and topographic attributes for mineralization. In most cases, these areas are surrounded by enhanced fault density and fault intersections, and these faults pass through the volcanic structures.

4.3. Distribution of mineral targets

Along the Mohn's Ridge, the predictive exploration model identified a total of 4,584 prospective targets representing approximate positions of first-order favorable sites to be investigated. Because (1) the model M3 has 22 control cells covering a maximum extent of 600 m, and (2) target points are generated at mid-way of this distance (300 m), a 300-m buffer distance is attributed to each of the target points to account the favorable surrounding environment. When target minerals are close, respective buffered zones agglomerate to form clusters (or target areas) where relevant evidential features are expected. In this context, most of the 4,584 prospective targets have been aggregated into 75 target areas of 2 or more targets, while 1 of these prospective areas correspond to a single target. The resulting 300-m-buffered target areas represent zones outlining limits of prediction where likelihood of mineralization is comparable to the Loki's Castle model. Because the targeting process depends entirely on the exploration model, a more detailed geological aspect of the model (i.e., more than 11 variables considered) could reduce the potential prospective areas.

The figure 5 displays potential SMS occurrences according to the minimum criteria established for target investigations (cf. section 2.5.1). The mineral targets are correlated with highly favorable zones in 20 neo-volcanic zones (among 34 delineated) that are usually set in continuous ridge sections. The target areas correspond to reduced extents of favorable areas (weighted above 2.20) and indicate about 141.12 km2 (5.70%) of high potential zones among the 2473.79 km2 covered in total by their respective neo-volcanic zones. In terms of findings, a target area does not necessarily describe single potential discovery since basalt-hosted vent occurrences may have widespread active and/or inactive extended vent systems at volcanic settings (e.g. Snake Pit vent field; Fouquet et al., 1993).

4.4. Numbers of undiscovered SMS deposits

Given the 2922.53 km2 of permissive area covering the ridge-valley floors, and a median tonnage of 0.9 Mt of analogue VMS deposits, we estimated by using the equations (Singer and Kouda, 2011) in Appendix C the number of undiscovered deposits at different prediction levels. The 90th percentile estimate is 3 or more, the 50th is 8 or more, and the 10th is 23 or more deposits. The expected number of deposits is 11 which is comparable to the predicted number of undiscovered vent fields along the Mohn's Ridge (i.e., 6) calculated by Beaulieu et al. (2015) on the basis of spreading rate and the global distribution of vents. Consecutive percentiles, standard deviation and mode were calculated (Table 8) based on the prediction levels assuming a lognormal distribution of numbers of deposits (Fig.6). The coefficient of variation (~81%; Table 8) displays a large variability between the higher and lower observations.

5. DISCUSSION

5.1. Weight characteristics

Although the previously defined methodology for component analysis presents an efficient weighting approach, the resulting weight coefficients (loadings) of the calculated component can be influenced by two major uncertainties: (1) the un-measured impact of using ternary values during the data analysis since the predictive values 0 are not included in the calculation of the covariance matrix and the loadings. This could constrain the spatial coverage of high scores and increase uncertainty in areas with unevaluated prediction; and (2) the definition and construction of evidence maps are adjusted according the characteristics of variables (Table 2 and 3), and thus depends in chosen pre-evaluation rules required by the ternary transformation. These rules result from empirical measures and observations and do not derive from e.g., simulation experiments; a simulation approach would quantify potential changes of a variable and related impact on hydrothermal activity and subsequent ore mineralization. Nevertheless, these uncertainties essentially affect areas beyond the limits of neo-volcanic zones. They have minor impact on final determination of exploration targets and no impacts on numbers of undiscovered deposits given that both are strictly based on the reference model.

5.2. Regional prospectivity mapping

A favorability value only represents likelihood of mineralization, and thus, areas outlined as having a low favorability need not necessarily to be ruled out for possible existence because the regional favorability map reflects exclusively the extracted data and the known vent field occurrence included in the analysis. Indeed, due to the possibility of finding off-axis sulfide deposits such as the TAG deposit associated to long-lived boundary faults and pillow volcanoes (Hannington et al., 1998), some deposits could fall outside the high favorability areas. In a regional context, as the mineralization potential is inherently probabilistic, we cannot speak of a cell belonging to a certain deposit type, especially from off-axis areas. However, the presence or the distance from the ridge axis gives a hint about, for example, the type of host-rock, especially if investigations are limited to the ridge valley. In comparison, the ridge walls are lithologically more diversified and must be investigated further in detail beyond a bathymetric map.

Nevertheless, off-axis areas with potential tectonic-related ore deposits remain prevalent in SMS exploration (e.g., those hosted in ultramafic rocks of detachment-fault systems; Petersen et al., 2009). Refining their geological characteristics and producing more indicative variables for further favorability calculations might result to a complete different picture of the prospectivity map. However, such study would require more reliable geoscience data to be compared with known SMS deposits along slow-spreading ridges. One might not necessarily identify the most useful geo-information when using topographical features since relevant geological processes for sulfide deposition often have hidden aspects (e.g. intrusion of magmatic bodies at rift flank transported off-axis during detachment faulting; Allen and Seyfried, 2004; McCaig et al., 2007; Petersen et al., 2009), and in this case, geophysical explorations are required.

5.3. Distribution of mineral targets

At the Mohn's Ridge, target areas are reported either at the crest or the flank of elongated axial domes generally subdivided by post-processed faults, at rifted valley zones or at the confluence of cross-cutting fault populations in volcano-tectonic terrains. Some of the target fields are directly comparable to the geological setting of vent fields at slow spreading ridges such as the Broken Spur and Snake Pit vent fields situated along elongated and fissured volcanic domes and spatially related to graben structures (Fouquet et al., 1993; Murton et al., 1994). Any potential hydrothermal activity depicted from the target areas can thus be controlled by a combination of recent volcanism and faulting.

Because the neo-volcanic zones tend to have various tectono-magmatic evolutions and configurations, we cannot dissociate, in most cases, magmatic and tectonic controls over the potential mineralization processes. In addition, some of the structural features analyzed may plausibly provide more (or less) favorable conditions for hydrothermal activity; e.g. a well-defined fault offset would suggest deep faulting and presumably allow the system to mine heat from a deep crustal source. In this regard, our methodology does not evaluate individual features but rather depict favorable structural environments with a variety of topographic and interpretive information.

5.4. Number of undiscovered SMS deposits

The estimated numbers of undiscovered deposits reflect the dependence of estimates with the delineation accuracy of the tracts. Mosier et al. (2007) demonstrated that estimates of deposit densities are inversely correlated with both the map scale and the size of the permissive tracts because larger areas result in overestimation of the permissive geology. In this study, the bathymetric map has a large scale (1:100,000), allowing delineation of permissive areas smaller than generally used for SMS density estimates (Singer, 2014; Hannington et al., 2011). Permissive areas with reduced size are more likely to exclude non-permissive rock units, resulting in higher deposit densities. In comparison, Hannington et al. (2011) tested similar regression approach on lower bathymetric scale map (1:2,500,000) and found an average of 18 deposits in control areas. This was done by counting prospects and occurrences rather than the well-defined and studied deposits used in the Singer (2014) study, and taking large uncertainties on permissive units on either side of mid-ocean ridges (50 km off distances) into account. On the other hand, Singer (2014) proposed more restrictive estimates along ridge axes evaluated at 2-km border sides, but with long and continuous spreading centers (64,000 km). He found at least 9 and 69 deposits for the 90th and 10th percentiles respectively, which is much lower than the estimates in this study considering the size difference of permissive areas involved (256,000 km2 versus 2,922 km2). Nevertheless, our approach uses more detailed geological inputs, as well as more restrictive spatial rulesets aimed to fit a deposit model already well established.

As these estimations may have direct economic implications, general considerations shall be made and summarized. First, the mineral resources are evaluated without including extinct deposits that may be buried by sediments on flattened and old seafloors, especially those in junction with the ridge flanks. Moreover, older crusts exceeding the

ridge valley floor limit are, as previously stated, not considered. Given the significant present-day discoveries far off-axis at the MAR (Fouquet et al., 2010), this raises the possibility of higher resource abundance that can be located and exploited in the more tectonic-oriented settings, where deposits are commonly hosted in systems with ultramafic basement.

Secondly, although permissive geology exists toward the southern Mohn's Ridge, the associated regional setting has shallower configuration and abnormally abundant volcanic activities. Any potential discoveries in these areas have to be investigated for economic purpose given that Zn-Cu type deposits associated to white smokers have been found further south on the Jan Mayen platform where they apparently develop in a shallow system with discharging fluids at temperature close to the boiling point (Pedersen et al., 2010).

Finally, the calculated deposit densities in this study are better used as guidelines to final estimates on the number of undiscovered deposits, due to the lack of reliable information on the spatial distribution of SMS deposits associated to active or inactive vent fields. Considerable information is available on VMS deposits known on land which can serve to make estimates as was done in this study. The equations used to estimate number of undiscovered deposits were based on well-explored control tracts on land (Singer, 2008; Singer and Kouda, 2011). In addition, the identified mineral targets cannot be accounted in these estimates because the identification process is exclusively model-based and requires additional reliable and informative targeting criteria. However, the probability that a particular target may represent one (or more) deposit cannot be ruled out since the target areas generally extend over high favorability zones inside the permissive tracts.

CONCLUSIONS

Data related to the SMS deposits have been collected based on topographic and geologic information, along an entire ultra-slow spreading ridge. After analyzing, extracting and combining the data, we have established in a probabilistic form, spatial relationships between morpho-structural features and mineral deposits. Though this paper has discussed several difficulties in applying threshold concepts to a dataset, it outlines further challenges and practice improvements to be made in computer-oriented exploration for seafloor mineral resources. In particular, the application of the characteristic analysis to a ridge-scale study of a portion of the AMOR system was successfully developed in a GIS framework to provide reasonable evaluation of prospective areas. It indicated the various characters of these areas

displaying interplays between volcanic and tectonic processes that are crucial ingredients for seafloor mineralization. Given that current research about SMS is still at the exploration stage, further discoveries may add baselines to finding potential survey targets prior to investigations.

The prediction process in this study narrowed the ridge-scaled exploration scope over 63 well-defined target areas, and specified an expected amount of 11 SMS deposits yet to be discovered in volcanic ridges. From an economic point of view, results obtained from the mineral targeting method cannot be considered for estimating the frequency distribution of undiscovered SMS deposits. Besides this, 2922.53 km2 of permissive tracts were delineated using consistent rules to provide reasonable input to make regression estimates of number of deposits. Importantly, the evaluation method used to find and evaluate the number of SMS deposits provides information more than ever necessary given the resources committed in present-day marine exploration, and the economic considerations driven by commercial interests. However, it should be remembered that mineral deposits have various sizes, adding further questions about the economic aspect of mining some of those that have yet to be discovered.

ACKNOWLEDGEMENTS

Much of the research is based on data provided by the Norwegian Petroleum Directorate (NPD). We acknowledge Prof. Georgy Cherkashev for providing additional geoscientific information, and Richard Sinding-Larsen for its critical reviews and constructive comments on the methodology applied. Two anonymous reviewers improved the quality of the manuscript with valuable comments and suggestions and are gratefully acknowledged.

REFERENCES

Abelson, M., Baer, G., Agnon, A., 2001. Evidence from gabbro of the Troodos ophiolite for lateral magma transport along a slow-spreading mid-ocean ridge. Nature, 409, 72–75.

Adamides, N., 2010a. Mafic-dominated volcanogenic sulphide deposits in the Troodos ophiolite, Cyprus Part 1–The deposits of the Solea graben. Applied Earth Science: Transactions of the Institutions of Mining and Metallurgy: Section B 119, 65-77.

Adamides, N., 2010b. Mafic-dominated volcanogenic sulphide deposits in the Troodos ophiolite, Cyprus Part 2–A review of genetic models and guides for exploration. Applied Earth Science: Transactions of the Institutions of Mining and Metallurgy: Section B 119, 193-204.

Allen,D.E., Seyfried,W.E.Jr., 2004. Serpentinization and heat generation: constraints from lost city and rainbow hydrothermal systems. Geochim Cosmochim Acta, 68, 1347 -1353.

Beaulieu, S.E., 2010. InterRidge Global Database of Active Submarine Hydrothermal Vent Fields, Version 2.0: http://www.interridge.org/irvents.

Beaulieu, S.E., Baker, E.T., German, C.R., and Maffei, A., 2013. An authoritative global database for active submarine hydrothermal vent fields. Geochem. Geophy. Geosy. 14,4892–4905.

Beaulieu, S.E., Baker, E.T., German, C.R., 2015. Where are the undiscovered hydrothermal vents on oceanic spreading ridges? Deep Sea Research Part II, 121. http://dx.doi.org/10.1016/j.dsr2.2015.05.001

Bruvoll, V., Breivik, A.J., Mjelde, R., Pedersen, R.B., 2009. Burial of the Mohn-Knipovich seafloor spreading ridge by the Bear Island Fan: Time constraints on tectonic evolution from seismic stratigraphy: Tectonic of the Mohn/Knipovich Bend. Tectonics, 28, TC4001. doi:10.1029/2008TC002396

Cann, J., Gillis, K., 2004. Hydrothermal insights from the Troodos ophiolite, Cyprus. Hydrogeol. Ocean. Lithosphere, 1, 272.

Cannat, M., Mangeney, A., Ondréas, H., Fouquet, Y., Normand, A., 2013. High-resolution bathymetry reveals contrasting landslide activity shaping the walls of the Mid-Atlantic Ridge axial valley: Landslides at axial valley walls. Geochem. Geophys. Geosystems, 14, 996–1011. doi:10.1002/ggge.20056

Canny, J., 1986. A Computational Approach to Edge Detection. IEEE Trans, Pattern Anal. Mach. Intell., 8 (6), 679-687.

Carbotte, S. M., Detrick, R. S., Harding, A., Canales, J. P., Babcock, J., Kent, G., van Ark, E., Nedimovic, M., Diebold, J., 2006. Rift topography linked to magmatism at the intermediate spreading Juan de Fuca Ridge. Geology, 34, (3), 2094212.

Chen,Y.J., 1992. Oceanic crustal thickness versus spreading rate, Geophys. Res. Lett., 19, 753–756. doi:10.1029/92GL00161

Cherkashov, G., Bel'tenev, V., Ivanov, V., Lazareva, L., Samovarov, M., Shilov, V., Stepanova, T., Glasby, G.P., Kuznetsov, V., 2008. Two New Hydrothermal Fields at the Mid-Atlantic Ridge. Mar. Georesources Geotechnol., 26, 308–316. doi:10.1080/10641190802400708

Clague, D. A., Moore, J. G. and Reynolds, J. R., 2000. Formation of submarine flat-topped volcanic cones in Hawai'i. Bulletin of Volcanology, 62 (3), 214-233.

Curewitz, D., and Karson, J.A., 1997. Structural settings of hydrothermal outflow: Fracture permeability maintained by fault propagation and interaction. J. Volcanol. Geotherm. Res., 79 (3-4), 149-168.

Dauteuil, O., Brun, J.-P., 1993. Oblique rifting in a slow-spreading ridge. Nature, 361, 145–148. doi:10.1038/361145a0

Dauteuil, O., and Brun, J.P., 1996. Deformation partitioning in a slow spreading ridge undergoing oblique extension: Mohns Ridge, Norwegian Sea. Tectonics, 15, 870–884.

Davis, J. C., 2002. Statistics and data analysis in geology (third edition). John Wiley and Sons, New York, 638.

Drummond, S.E., Ohmoto, H., 1985. Chemical Evolution and Mineral Deposition on Boiling Hydrothermal Systems. Economic Geology, 80, 126-147.

Duda, R.O., Hart, P.E., 1972. Use of the Hough transformation to detect lines and curves in pictures. Communications of the ACM, 15 (1), 11-15.

Eilu, P., Rasilainen, K., Halkoaho, T., Huovinen, I., Kärkkäinen, N., Kontoniemi, O., Lepistö, K., Niiranen, T. and Sorjonen-Ward, P., 2015. Quantitative assessment of undiscovered resources in orogenic gold deposits in Finland. Geological Survey of Finland, Report of Investigation 216, 2015.

Ellefmo, S., Sinding-Larsen, R., Søreide, F., 2017. Ancient, recent and future yet-to-find mineral resource assessments along the AMOR. Norsk Geologisk Winter Conference 2017, Oslo.

Fouquet, Y., Wafik, A., Cambon, P., Mevel, C., Meyer, G., Gente, P., 1993. Tectonic setting and mineralogical and geochemical zonation in the Snake Pit sulfide deposit (Mid-Atlantic Ridge at 23°N). Economic Geology, 88, 2018–2036.

Fouquet, Y., Cambon, P., Etoubleau, J., Charlou, J.L., Ondréas, H., Barriga, F.J.A.S., Cherkashov, G., Semkova, T., Poroshina, I., Bohn, M., Donval, J.P., Henry, K., Murphy, P., Rouxel, O., 2010. Geodiversity of hydrothermal processes along the Mid-Atlantic Ridge and ultramafic-hosted mineralization: A new type of oceanic Cu-Zn-Co-Au volcanogenic massive sulfide deposit, in: Rona, P.A., Devey, C.W., Dyment, J., Murton, B.J. (Eds.), Geophysical Monograph Series. American Geophysical Union, Washington, D. C., 321–367.

Fournier, M., and Petit, C., 2007. Oblique rifting at oceanic ridges: Relationship between spreading and stretching directions from earthquake focal mechanisms. J. Struct. Geol., 29, 201–208. doi:10.1016/j.jsg.2006.07.017

Galley, A.G. and Koski, R.A., 1999. Setting and characteristics of ophiolite-hosted volcanogenic massive sulphide deposits." Reviews in Economic Geology 8: 215-236.

Géli, L., Renard, V., Rommevaux, C., 1994. Ocean crust formation processes at very slow spreading centers: A model for the Mohns Ridge, near 72°N, based on magnetic, gravity, and seismic data. Journal of Geoph. Res., 99, 2995-3013. doi: 0148-0227/94/9 3JB-02966505.00

Germanovich, L. N., Lowell, R. P., and Astakhov, D. K., 2000. Stress-dependent permeability and the formation of seafloor event plumes, J. Geophys. Res., 105(B4), 8341-8354.

Haase, K.M., Petersen, S., Koschinsky, A., Seifert, R., Devey, C.W., Keir, R., Lackschewitz, K.S., Melchert, B., Perner, M., Schmale, O., Süling, J., Dubilier, N., Zielinski, F., Fretzdorff, S., Garbe-Schönberg, D., Westernströer, U., German, C.R., Shank, T.M., Yoerger, D., Giere, O., Kuever, J., Marbler, H., Mawick, J., Mertens, C., Stöber, U., Walter, M., Ostertag-Henning, C., Paulick, H., Peters, M., Strauss, H., Sander, S., Stecher, J., Warmuth, M., Weber, S., 2007. Young volcanism and related hydrothermal activity at 5°S on the slow-spreading southern Mid-Atlantic Ridge: Young Volcanism and Hydrothermal Activity. Geochem. Geophys. Geosystems, 8. doi:10.1029/2006GC001509

Hannington, M.D., Galley, A.G., Herzig, P.M., Petersen, S., 1998. Comparison of the TAG mound and stockwork complex with Cyprus-type massive sulfide deposits. Proc. Ocean Drill. Program Sci. Results, 158, 389–415.

Hannington, M.D., de Ronde, C.D., Petersen, S., 2005. Sea-floor tectonics and submarine hydrothermal systems. Society of Economic Geologists, Inc. Economic Geology 100th Anniversary Volume, 111–141.

Hannington, M., Jamieson, J., Monecke, T., Petersen, S., 2010. Modern sea-floor massive sulfides and base metal resources: toward an estimate of global sea-floor massive sulfide potential. Soc. Econ. Geol. Spec. Publ., 15, 317–338.

Hannington, M.D., Jamieson, J., Monecke, T., Petersen, S., and Beaulieu, S., 2011. The abundance of seafloor massive sulfide deposits: Geology, 39 (12), 1155-1158.

Jowitt, S.M., McEvoy, F.M., Williamson, J.P., Bateson, L., Naden, J., Gunn, A.G., Nicolaides, S., 2005. Mineralisation potential mapping for ophiolite-hosted volcanic massive sulphide (VHMS) deposits, Troodos Ophiolite, Cyprus. In: Mao, J., Bierlein, F.P. (ed.) Mineral Deposit Research: Meeting the Global Challenge, 2, 1469-1473.

Karson, J.A. and Rona, P.A., 1990. Block-tilting, transfer faults and structural control of magmatic and hydrothermal processes in the TAG area, Mid-Atlantic Ridge 26°N. Geological Society of America Bulletin, 102, 1635–1645.

Kelley, D.S., 2005. A Serpentinite-Hosted Ecosystem: The Lost City Hydrothermal Field. Science, 307, 1428–1434. doi:10.1126/science.1102556

Klingelhofer, F., Geli, L., Matias, L., Steinsland, N., Mohr, J., 2000. Crustal structure of a super-slow spreading centre: a seismic refraction study of Mohns Ridge, 72 N. Geophys. J. Int., 141, 509–526. doi:10.1046/j.1365-246x.2000.00098.x

Langmuir, C., Humphris, S., Fornari, D., Van Dover, C., VonDamm, K., Tivey, M.K., Colodner, D., Charlou, J.L., Desonie, D., Wilson, C., Fouquet, Y., Klinkhammer, G., and Bougault, H., 1997. Hydrothermal vents near a mantle hot spot: The Lucky Strike vent field at 37°N on the Mid-Atlantic Ridge, Earth Planet. Sci. Lett., 148, 69–91. doi:10.1016/S0012-821X(97)00027-7

Large, R.R., 1992. Australian volcanic-hosted massive sulfide deposits: features, styles, and genetic models. Economic Geology, 87 (3), 471-510.

Li, B., Shi, X., Yang, Y., Ye, J., Gao, J., Zheng, W., 2014. Geochemistry of mafic rocks and melt inclusions and their implications for the heat source of the 14.0°S hydrothermal field, South Mid-Atlantic Ridge. Chin. J. Geochem., 33, 325–335. doi:10.1007/s11631-014-0695-x

McCaig, A.M., Cliff, R.A., Escartin, J., Fallick, A.E., MacLeod, C.J., 2007. Oceanic detachment faults focus very large volumes of black smoker fluids. Geology, 35, 935. doi:10.1130/G23657A

McCammon, R.B., Botbol, J.M., Sinding-Larsen, R., Bowen, R.W., 1983. Characteristics analysis – 1981: final program and a possible discovery. Mathematical Geology, 15 (1), 59-83.

Mendel, V., Sauter, D., Rommeveaux-Jestin, C., Patriat, P., Lefebvre, F., and Parson, L.M., 2003. Magmato-tectonic cyclicity at the ultra-slow spreading Southwest Indian Ridge: Evidence from variations of axial volcanic ridge morphology and abyssal hills pattern. Geochem. Geophys. Geosyst., 4 (5), 9102. doi:10.1029/2002GC000417

Monecke, T., Petersen, S., Hannington, M.D., 2014. Constraints on water depth of massive sulfide formation: evidence from modern seafloor hydrothermal systems in arc-related settings. Econ. Geol., 109, 2079–2101.

Moores, E.M., and Vine, F.J., 1971. The Troodos massif, Cyprus and other ophiolites and oceanic crust: evaluation and implications. Royal. Soc. London Philos. Trans. A., 268, 443–466.

Mosier, D.L., Singer, D.A., and Berger, V.I., 2007. Volcanogenic massive sulfide deposit density. U.S. Geological Survey Scientific Investigations Report, 2007-5082.

Mosier, D.L., Berger, V.I., and Singer, D.A., 2009, Volcanogenic massive sulfide deposits of the world; database and grade and tonnage models: U.S. Geological Survey Open-File Report 2009-1034.

Münch, U., Halbach, P., Fujimoto, H., 2000. Sea-floor hydrothermal mineralization from the Mt. Jourdanne, Southwest Indian Ridge. Jamstec J Deep Sea Res, 16.

Murton, B.J., Klinkhammer, G., Becker, K., Briais, A., Edge, D., Hayward, N., Millard, N., Mitchell, I., Rouse, I., Rudnicki, M., Sayanagi, K., Sloan, H., Parson, L., 1994. Direct evidence for the distribution and occurrence of hydrothermal activity between 27°N–30°N on the Mid-Atlantic Ridge. Earth Planet. Sci. Lett., 125, 119–128. doi:10.1016/0012-821X(94)90210-0

Neumann, E.G., and Schilling, J.G., 1984. Petrology of basalts from the Mohns-Knipovich Ridge, the Norwegian-Greenland Sea, Contrib. Mineral. Petrol., 85, 209–223.

Parson, L.M., Murton, B.J., Searle, R.C., and Walker, C., 1993. En echelon axial volcanic ridges at the Reykjanes Ridge: a life cycle of volcanism and tectonics. Earth planet. Sci. Lett., 117, 73–87.

Pearce, J.A., and Robinson, P.T., 2010. The Troodos ophiolitic complex probably formed in a subduction initiation, slab edge setting. Gondwana Research, 18, 60-81.

Pedersen, R.B., Thorseth, I.H., Nygård, T.E., Lilley, M.D., Kelley, D.S., 2010. Hydrothermal activity at the Arctic mid-ocean ridges, in: Rona, P.A., Devey, C.W., Dyment, J., Murton, B.J. (Eds.), Geophysical Monograph Series. American Geophysical Union, Washington, D. C., 67–89.

Peirce, C., and Sinha, M. C., 2008. Life and death of axial volcanic ridges: segmentation and crustal accretion at the Reykjanes Ridge. Earth and Planetary Science Letters, 274 (1–2).

Pertsev, A.N., Bortnikov, N.S., Vlasov, E.A., Beltenev, V.E., Dobretsova, I.G., and Ageeva, O.A., 2012. Recent Massive Sulfide Deposits of the Semenov Ore District, Mid-Atlantic Ridge, 13°31' N: Associated Rocks of the Oceanic Core Complex and Their Hydrothermal Alteration. Geology of Ore Deposits, 54 (5), 334-346.

Petersen, S., Kuhn, K., Kuhn, T., Augustin, N., Hékinian, R., Franz, L., Borowski, C., 2009. The geological setting of the ultramafic-hosted Logatchev hydrothermal field (14°45'N, Mid-Atlantic Ridge) and its influence on massive sulfide formation. Lithos 112 (1), 40-56.

Rautenschlein, M., Jenner, G.A., Hertogen, J., Hofmann, A.W., Kerrich, R., Schmincke, H.-U., White, W.M., 1985. Isotopic and trace element composition of volcanic glasses from the Akaki Canyon, Cyprus: implications for the origin of the Troodos ophiolite. Earth and Planetary Science Letters 75, 369-383.

Rona, P.A., Hannington, M.D., Raman, C.V., Thompson, G., Tivey, M.K., Humphris, S.E., Lalou, C., Petersen, S., 1993. Active and relict seafloor hydrothermal mineralization at the TAG hydrothermal field, Mid-Atlantic Ridge. Econ. Geol., 18, 1989-2017.

Schilling, J.G., Kingsley, R., Fontignie, D., Poreda, R., and Xue, S., 1999. Dispersion of t he Jan Mayen and Iceland mantle plumes in the Arctic: A He-Pb-Nd-Sr isotope tracer study of basalts from the Kolbeinsey, Mohns, and Knipovich Ridges, J. Geophys. Res., 104, 10543–10569.

Shaw, P.R., Lin, J., 1993. Causes and consequences of variations in faulting style at the Mid-Atlantic ridge. Journal of Geoph. Res., 98, 21839-21851

Shaw, W.J., and Lin, J., 1996. Models of ocean ridge lithospheric deformation: Dependence on crustal thickness, spreading rate, and segmentation. Journal of Geophysical Research, 101, 17977–17993.

Singer, D.A., 1993. Basic concepts in three-part quantitative assessments of undiscovered mineral resources. Non-Renewable Resources, 2 (2), 69–81.

Singer, D.A., Menzie, W.D., Sutphin, D.M., Mosier, D.L., Bliss, J.D., 2001. Mineral deposit density: An update, chapter A of Schulz, K.J., ed., Contributions to global mineral resource assessment research: U.S. Geological Survey Professional Paper 1640, A1-A13 (also available online at https://pubs.usgs.gov/prof/p1640a/).

Singer, D.A., 2008. Mineral Deposit Densities for Estimating Mineral Resources. Math. Geosci., 40, 33–46. doi:10.1007/s11004-007-9127-3

Singer, D. A. and Menzie, W. D., 2010.Quantitative mineral resource assessments: An integrated approach. New York: Oxford University Press.

Singer, D.A., Kouda, R., 2011. Probabilistic Estimates of Number of Undiscovered Deposits and Their Total Tonnages in Permissive Tracts Using Deposit Densities. Nat. Resour. Res., 20, 89–93. doi:10.1007/s11053-011-9137-1

Singer, D.A., 2014. Base and precious metal resources in seafloor massive sulfide deposits. Ore Geol. Rev. 59, 66–72. doi:10.1016/j.oregeorev.2013.11.008

Smith, D. K., and Cann, J. R., 1990. Hundreds of small volcanoes on the median valley floor of the Mid-Atlantic Ridge. Nature, 348, 152–155. doi:10.1038/348152a0

Smith, D.K., Escartín, J., Schouten, H., Cann, J.R., 2008. Fault rotation and core complex formation: Significant processes in seafloor formation at slow-spreading mid-ocean ridges (Mid-Atlantic Ridge, 13°-15°N): Fault Rotation and Core Complex Formation. Geochem. Geophys. Geosystems, 9, Q03003. doi:10.1029/2007GC001699

Stensgaard, B.M., Kalvig, P., and Stendal, H., 2009. Quantitative Mineral Resource Assessment: Sedimentary-hosted Copper in Greenland: Reporting the Copper Assessment Workshop, GEUS, Copenhagen, March 2009.

Torsvik, T.H., Mosar, J., and Eide, E.A., 2001. Cretaceous-Tertiary geodynamics: a North Atlantic exercise: Geophysical Journal International, 146, 850–866.

Vogt, P.R., 1986. The present plate boundary configuration, in: Vogt, P.R., and Tucholke, B.E. (eds.), The Geology of North America, Volume M: The Western North Atlantic Region. Geological Society of America, Boulder, CO, 189-204.

Webber, A.P., Roberts, S., Murton, B.J., Hodgkinson, M.R.S., 2015. Geology, sulfide geochemistry and supercritical venting at the Beebe Hydrothermal Vent Field, Cayman Trough: Beebe hydrothermal vent field geology. Geochem. Geophys. Geosystems 16, 2661–2678. doi:10.1002/2015GC005879

Wheeler, A.J., Murton, B., Copley, J., Lim, A., Carlsson, J., Collins, P., Dorschel, B., Green, D., Judge, M., Nye, V., Benzie, J., Antoniacomi, A., Coughlan, M., Morris, K., 2013. Moytirra: Discovery of the first known deep-sea hydrothermal vent field on the slow-spreading Mid-Atlantic Ridge north of the Azores. Geochem. Geophys. Geosystems, 14, 4170–4184. doi:10.1002/ggge.20243

Yeo, I., Searle, R.C., Achenbach, K.L., Le Bas, T.P., Murton, B.J., 2012. Eruptive hummocks: Building blocks of the upper ocean crust. Geology, 40, 91–94.

Appendix A. Favorability calculation

Assuming the matrix X containing the data of *n* observations and *m* variables, any favorability value can be denoted as x_{ij}. A variable *j* favorable to cell *i* will provide +1, -1 if unfavorable or 0 if unevaluated. Corresponding weights of ternary-transformed variables are determined by solving the matrix equation (McCammon et al., 1983):

$$(X'X)a = \lambda a \quad (1)$$

where λ corresponds to the largest eigenvalue of the covariance matrix ($X'X$), and a represents the largest eigenvector (principal component) associated with λ that show the greatest variance in the dataset. The a_i (i =1,2,…,n) are elements of the eigenvector and describe the weight coefficients of the combined geological variables (Table 3).

A favorability value f can then be calculated for a given cell from a weighted linear combination of the ternary-transformed variables:

$$f = a_1x_1 + a_2x_2 + \cdots + a_nx_n \quad (2)$$

where x_i represents the n transformed variables. Because mineral exploration commonly requires different combination of variables with respect to a deposit model, variables dependency shall be defined by the means of logical combinations AND, OR and NOT (McCammon et al., 1983). Expert judgment of the deposit model is essential to describe particular combinations as favorable or unfavorable. In consequence, the observations x_i include both the ternary-transformed variables and their logical combinations. This approach allows improvement of the results obtained from the CA when calculating values from f.

One significant logical combination of exploration data is based on the relationship between the distance from the ridge axis, the presence of the neo-volcanic zones and the other variables. Indeed, as shown by Beaulieu (2010), almost all discovered SMS deposits have strong spatial and temporal correlation with magmatism along MORs. This genetic and spatial relationship is fundamental for exploration targeting of vent fields along these ridges because the underlying heat source tends to be attenuated with distance from the ridge axis. Depending on the criteria associated to the distance from the ridge axis (i.e. variable *R_DIST* in table 3), any other variable may be transformed into -1 if they fall in conditions that tend to be unfavorable. Therefore, cells of any evidence map evaluated to be too far away from the ridge axis and the neo-volcanic zones obtain negative values.

Appendix B. Model generalization

McCammon et al. (1983) described the problem that arises in defining regionalized models based on selected cells. Indeed, regional cells selected for M2 can be determined to have same or greater degrees of match with the restrictive model M1 than contains only known deposits. However, it is uncertain whether this degree of match is completely due

to chance or whether there exists a significant relationship between the cells of M1 and M2. For this reason, we calculate the probability of chance that variables of each cell have similar patterns of occurrence, i.e. if their ternary values have similar arrangements in their degrees of matching. A variable can be defined as a sequence of ternary values, e.g. {1,0,1,1,-1,0,…,1,-1}, depending on the number of observations. For such variables, if we assume that the sequences of values of two variables have occurred randomly, we may determine whether the number of matches between these two sequences is a chance of occurrence or not. This can be done by calculating the probability mass function of discrete random variables between paired sequences to obtain the probability that a certain number of matches may correspond to another number of matches for sequences arranged in random orders (cf. McCammon et. al. 1983 for the expression of this probability). In this context, similar and dissimilar patterns correspond to high and low probabilities that the observed matches are not due to chance respectively.

If we consider M, a symmetric matrix n x n containing these probabilities, the cross-product expression X'X from (1) can be replaced by M, and weight coefficients (a_i) can be thereafter calculated. Favorability values *f* are then calculated, and cells of M2 that are highly favorable are selected. This model generalization has the advantage of not being exclusively restricted to the features that characterize the cells of M1.

Appendix C. Estimating the number of undiscovered deposits

Singer and Kouda (2011) developed a regressing model aimed at estimating probabilistically the number of undiscovered deposits, by regressing permissive areas, and median log-transformed tons in deposits, against density of deposits. By doing so, estimates are produced in probabilistic terms by establishing prediction limits to reduce related standard biases from the regression model:

$$R_{50} = 4.2096 - 0.4987\, log_{10} area - 0.2252\, log_{10} size \quad (3)$$

$$L_{90}, U_{10} = R_{50} \pm t\, S_{y|s,a} \sqrt{\left(\frac{1 + 1/n + (3.175 - log_{10}\, area)^2 (-0.3292 - log_{10}\, size)^2}{(n-1) S_s S_a}\right)} \quad (4)$$

where R_{50} corresponds to the 50th percentile in the estimates of deposit density (deposit per 100,000 km2), L_{90} and U_{10} represent the 90th and 10th percentiles respectively for the density of deposits, t is the Student's t parameter, $S_{y|s,a}$ is the

standard deviation of logarithmic values of deposit density given permissive area and deposit size, n is the number of permissive tracts studied worldwide, 3.175 is the mean logarithmic values of permissive tract area in square kilometers,-0.3292 is mean of logarithmic values of deposit tonnage in millions on metric tons in control tracts, 2.615 is the standard deviation of log-transformed deposit tonnages in permissive tracts, and 1.188 is standard deviation of logarithmic values of area of permissive tracts.

Our estimates are calculated for the total permissive area outlined from the neo-volcanic zones, and not for each tract thereafter aggregated because, as the general size of the permissive tracts is relatively small (Table 6), their related deposit density estimated would give rather high values. This would be a clear reflection of the inverse correlation of estimates of deposit densities with the size of the permissive tracts stated by Mosier et al. (2007).

As the estimates from the equations (3) and (4) are initially re-scaled for 100,000 km2, densities are thus adjusted for the size of the tracts by multiplying them with the factor $permissive\ area\ /\ 100{,}000\ km2$. Estimates on the number of deposits can then be calculated at the three different percent levels, using the estimated values as exponents to the power of 10:

$$N = (permissive\ area/100{,}000) * 10^{\log_{10}(Density)} \quad (5)$$

As one SMS deposit is known in one of our tracts, the calculated percentiles have been adjusted such that the known number of deposits is subtracted from the expected number by using the variance and the expected number of deposits from the regression model (Singer and Kouda, 2011):

$$var_N = ((log_{10}(N_{10}) - log_{10}(N_{50}))\ /\ t\ )^2 \quad (6)$$

$$log_{10}(N_{50}) = log_{10}\left(10^{E(N)} - known\ number\right) - var_N/2 \quad (7)$$

The resulting value of $log_{10}(N_{50})$ can be used as a revised estimate in place of R_{50} in the equation (3). The expected number of deposits $E(N)$ in the equation (7) corresponds to the mean of N considering N_{50} as log-normally distributed. It can be obtained as 10 of the power of:

$$log_{10}E(N) = log_{10}(N_{50}) + \left(\left(\left(log_{10}(N_{10}) - log_{10}(N_{50})\right) / t\right)^2\right) / 2 \quad (8)$$

Table 1. Information about SMS occurrences along the Mohn's Ridge (Pedersen et al., 2010).

Name	Longitude	Latitude	Depth (m)	Activity	Extent	Location
Loki's Castle	08°09′E	73°33′N	2400	Active	2 mounds ≥150 m in diameter	Crest of an AVR
Mohn 's Treasure	07°12′E	73°27′N	2600	Extinct	-	Off-axis, on a low-angle inner-valley fault
Copper Hill	02°10′E	72°32′N	900	Extinct	-	Off-axis, in a core complex terrain

Table 2. Characteristics of the prediction model for SMS deposits.

Information type	Prospective criteria	Characteristics
Terrain information	Slope	Favorable range of slope gradient
	Scarps	Favorable presence
	Depth	Favorable range of depth
	Ridge axis	Proximity
Morpho-structural information	AVRs	Favorable presence + proximity
	Volcanoes	Proximity + density
	Faults	
	Fault intersections	

Table 3. Exploration dataset input into a GIS for the Mohn's Ridge. Favorability criteria for the occurrence of SMS deposits in neo-volcanic zones are assigned to geological variables depending on specified spatial rules. Raster resolution is 50m (1:100,000 map scale).

Variables	Description	Favorable criterion	Unevaluated or uncertain criterion	Unfavorable criterion
AVR	Axial Volcanic Ridge (AVR) zone delineated from hummocky terrain and contour line distortion	On the AVR zone	Not on AVR zone	-
R_DIST	Distance from neo-volcanic ridge axis	Ranges to 3 km	Ranges from 3 to 8 km	Above 8 km
F_DIST	Distance from fault zone	Ranges to 200 m	Ranges from 200 to 500 m	Above 500 m

F_KD	Kernel density of fault zones (%) calculated to include all features within 2,000 m (search radius)	20% or above	Between 20% and 10%	Below 10%
FI_DIST	Distance from faults intersection	Ranges to 500 m	Above 500 m	-
FI_KD	Kernel density of fault intersections (%) with search radius of 2,000 m	20 % or above	Between 20% and 10%	Below 10%
VOLC_DIST	Distance from volcanic structures	Ranges to 1 km	Above 1 km	-
VOLC_KD	Kernel density of volcanic structures (%) with search radius of 2,000 m	15 % or above	Between 15% and 5%	Below 5%
SLOPE	Slope angle calculated from bathymetry data	32° or lower	Above 32°	-
SCARP	Scarps obtained from highest slope angles and aspect	On scarp	Not on scarp	-
DEPTH	Water depth	-1500 m or lower	Between -1500 m and -852 m	Above -852 m

Table 4. Averaged proximal distances estimated among geological features.

Feature	Mean proximity (m)	Standard deviation of proximity (m)
Fault	1683	1748
Fault intersect	1050	928
Volcano	2056	1479

Table 5. Weight values calculated for the models M1, M2 and M3.

Variables	M1	M2	M3
Nb. of cells	2	69	22
AVR	0.333	0.246	0.321
R_DIST	0.333	0.246	0.321
F_DIST	0.000	0.510	0.153
F_KD	0.333	0.246	0.321
FI_DIST	0.000	0.506	0.226

FI_KD	0.333	0.246	0.321
VOLC_DIST	0.333	0.246	0.321
VOLC_KD	0.333	0.246	0.321
SLOPE	0.333	0.000	0.321
SCARP	0.333	0.246	0.321
DEPTH	0.333	0.246	0.321
Cumulative total	2.997	2.984	3.268

Table 6. Statistics of the permissive tracts.

Count	Min. (km2)	Max. (km2)	Sum (km2)	Mean (km2)	Std. Dev. (km2)
34	3.05	266.53	2922	85.96	74.29

Table 7. Example of characteristic weights of variables calculated for a high regional favorability.

Variables	Characteristic weights
AVR	0.434
R_DIST	0.276
F_DIST	0.333
F_KD	0.351
FI_DIST	0.287
FI_KD	0.390
VOLC_DIST	0.333
VOLC_KD	0.345
SLOPE	0.026
SCARP	0.187
DEPTH	0.015
Cumulative total	2.977

Table 8. Estimated densities and number of undiscovered SMS deposits in neo-volcanic areas along the Mohn's Ridge.

	SMS density (dep./km2)	Number of deposits or more (rounded off to the upper limit)
Mode	0.0014	4
Mean	0.0037	11

Std. Dev.	-	9
Coef. Var.	-	0.81
F100	0.0003	1
F95	0.0007	2
F90	0.001	3
F75	0.0016	5
F50	0.0027	8
F25	0.0047	14
F10	0.0077	23
F5	0.0102	30
F0	0.0224	66

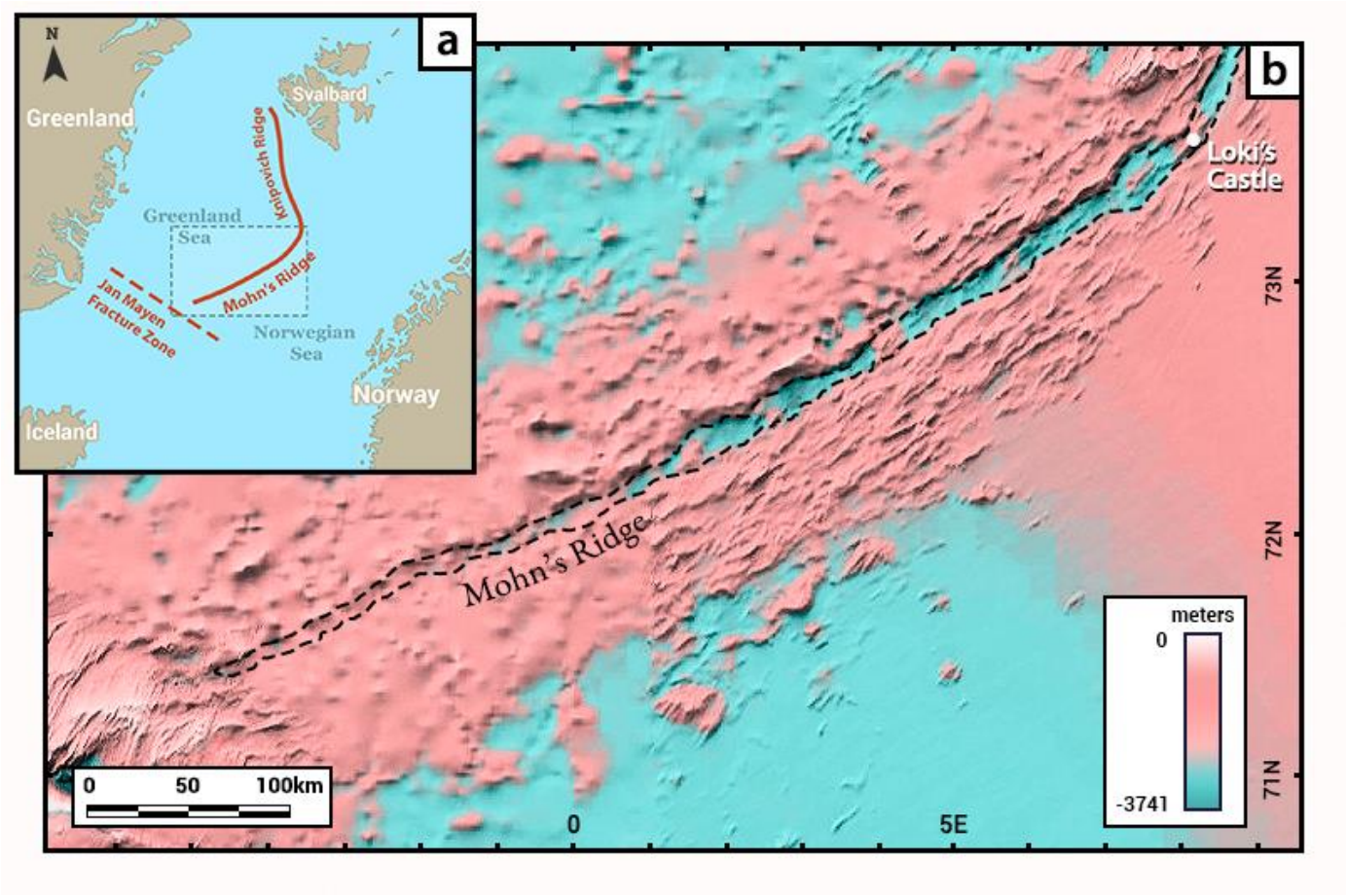

Fig. 1. (a) Map sketch and (b) bathymetry of the Mohn's Ridge. The black dashed lines delineate the ridge valley and the Loki's Castle vent field is shown at the northernmost part of the ridge. The basemap with shaded relief was taken

and modified from the GEBCO database (available at

http://www.gebco.net/data_and_products/gridded_bathymetry_data/).

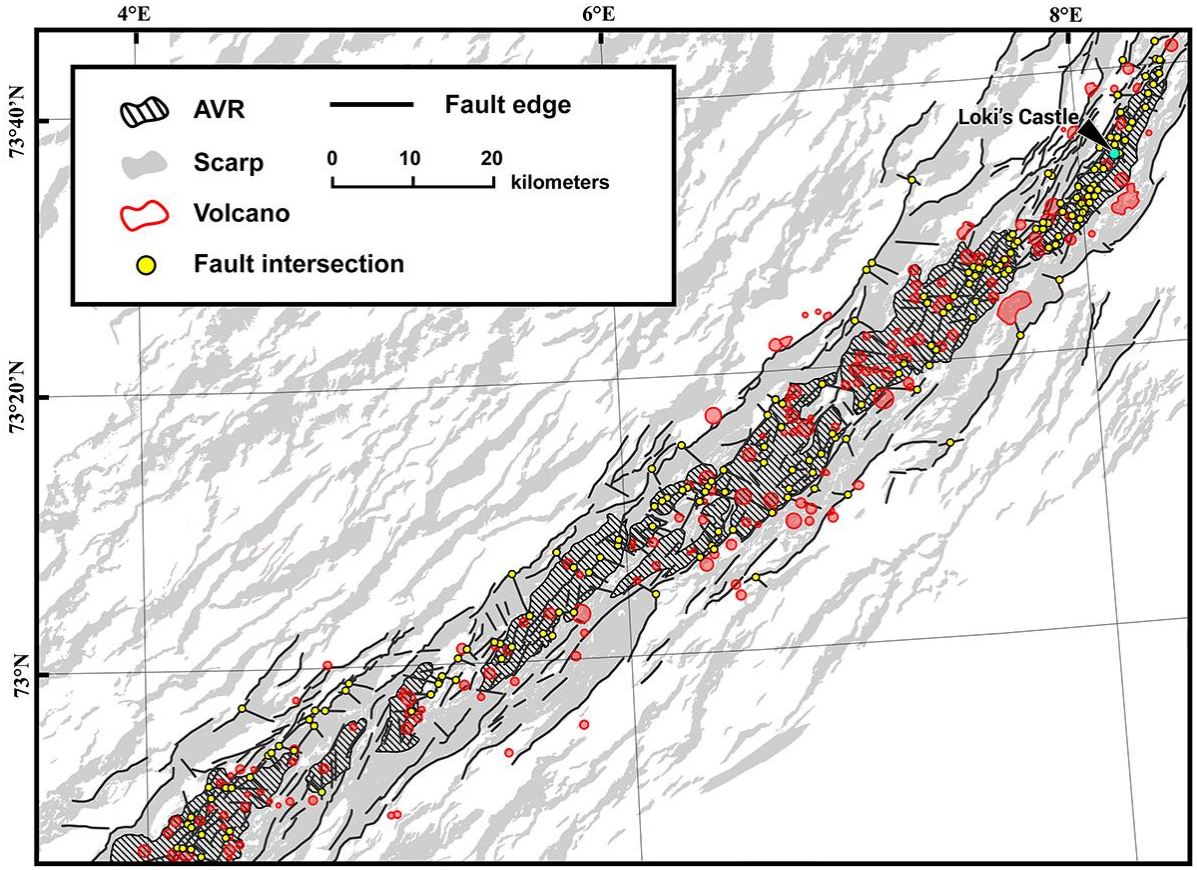

Fig. 2. Morpho-structural mapping of the faults, fault intersections, scarps, AVRs and volcanoes at the northern region of the Mohn's Ridge. The Loki's Castle vent field is shown at the northernmost part of the ridge.

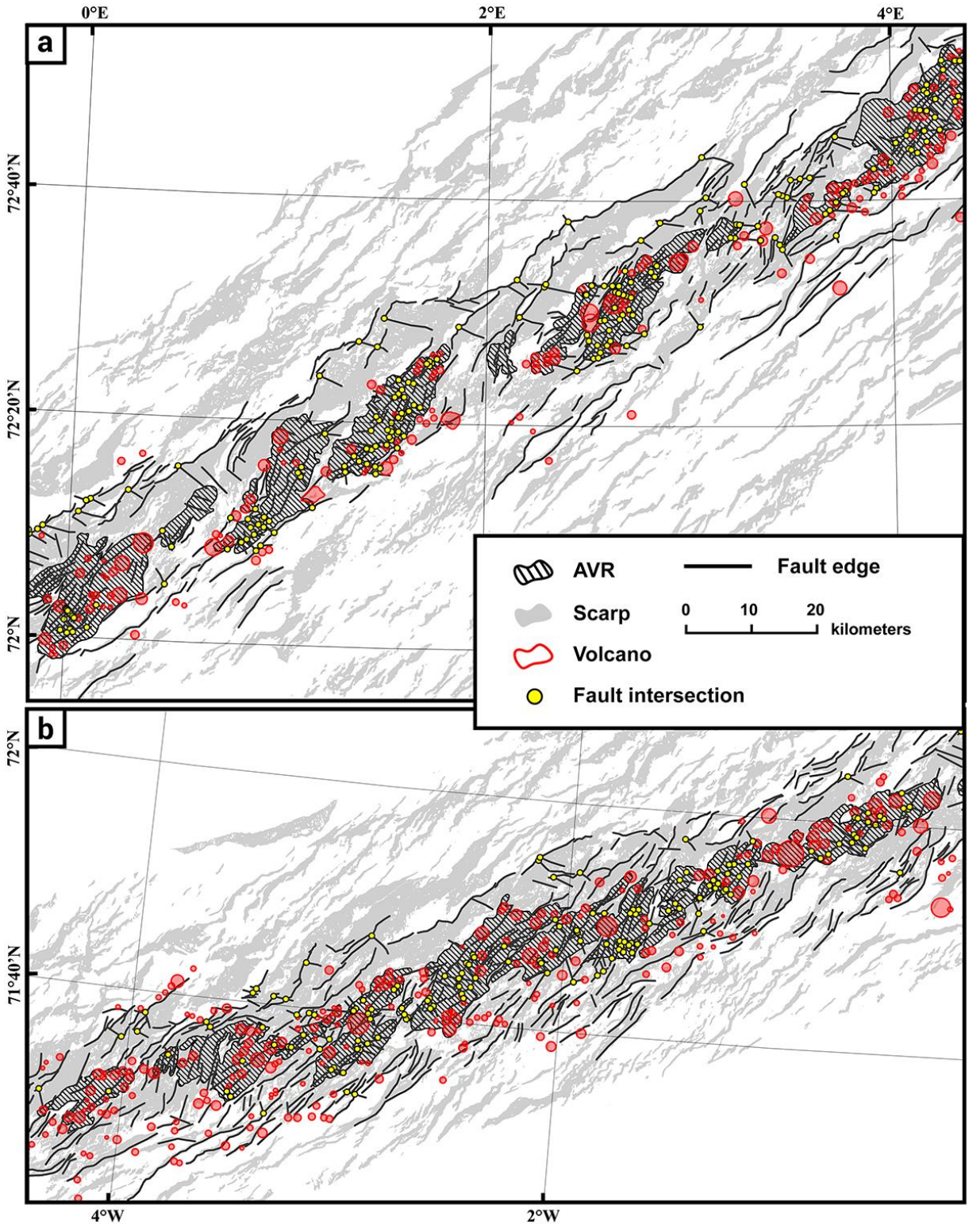

Fig. 3. Morpho-structural mapping of the faults, fault intersections, scarps, AVRs and volcanoes at midway (a) and southern (b) valley of the Mohn's Ridge.

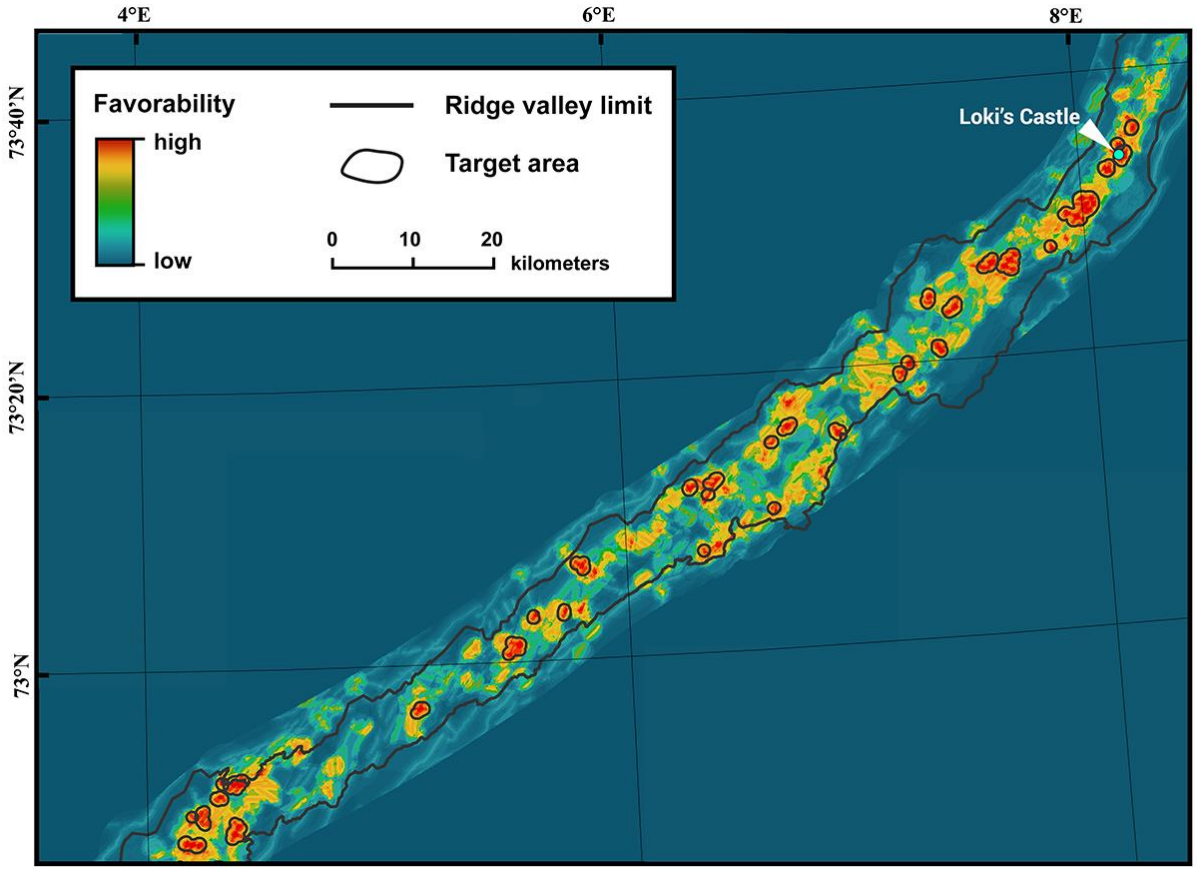

Fig. 4. Favorability map and target areas at the northern region of the Mohn's Ridge. The Loki's Castle vent field is shown at the northernmost part of the ridge.

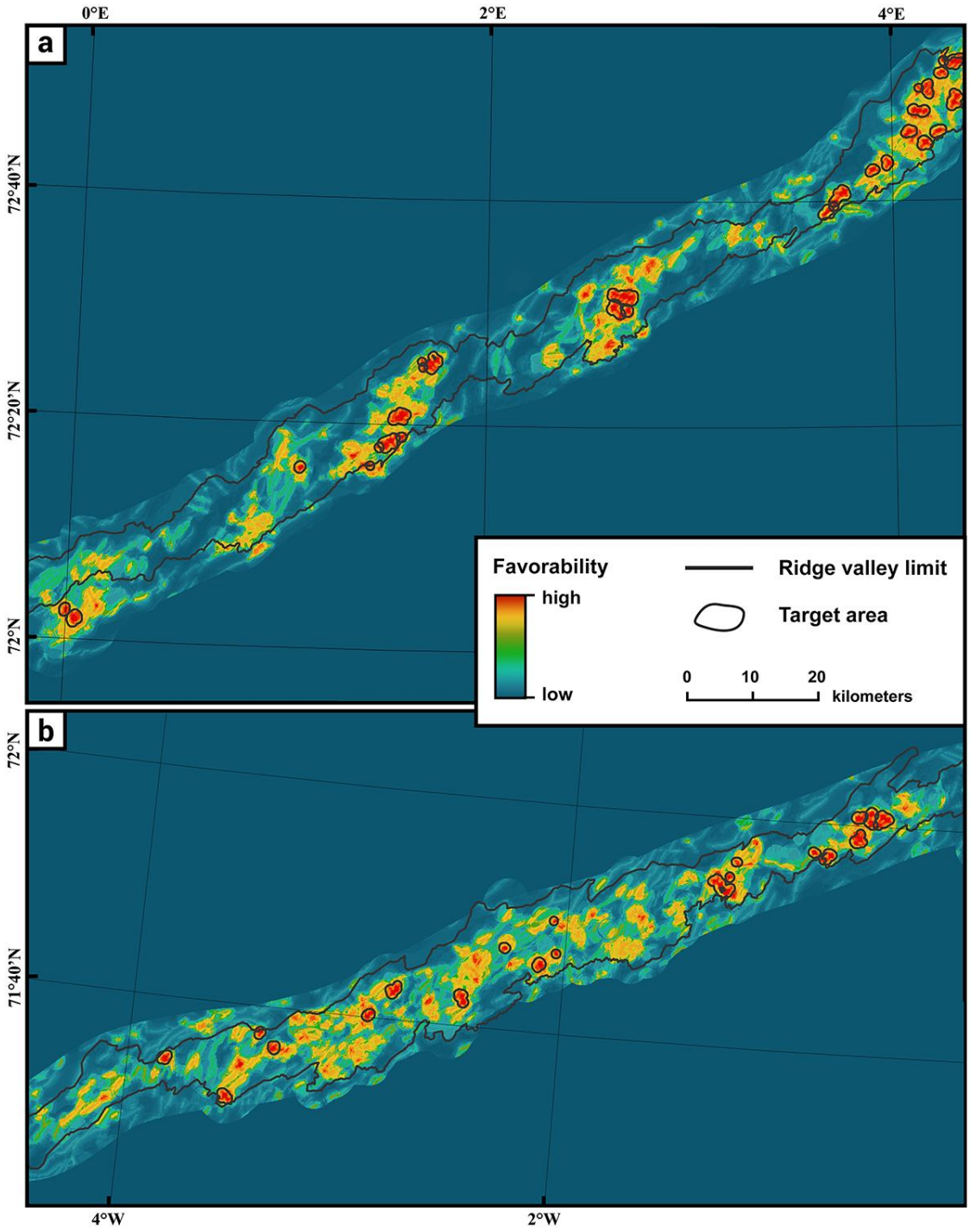

Fig. 5. Favorability map and target areas at midway (a) and southern (b) valley of the Mohn's Ridge.

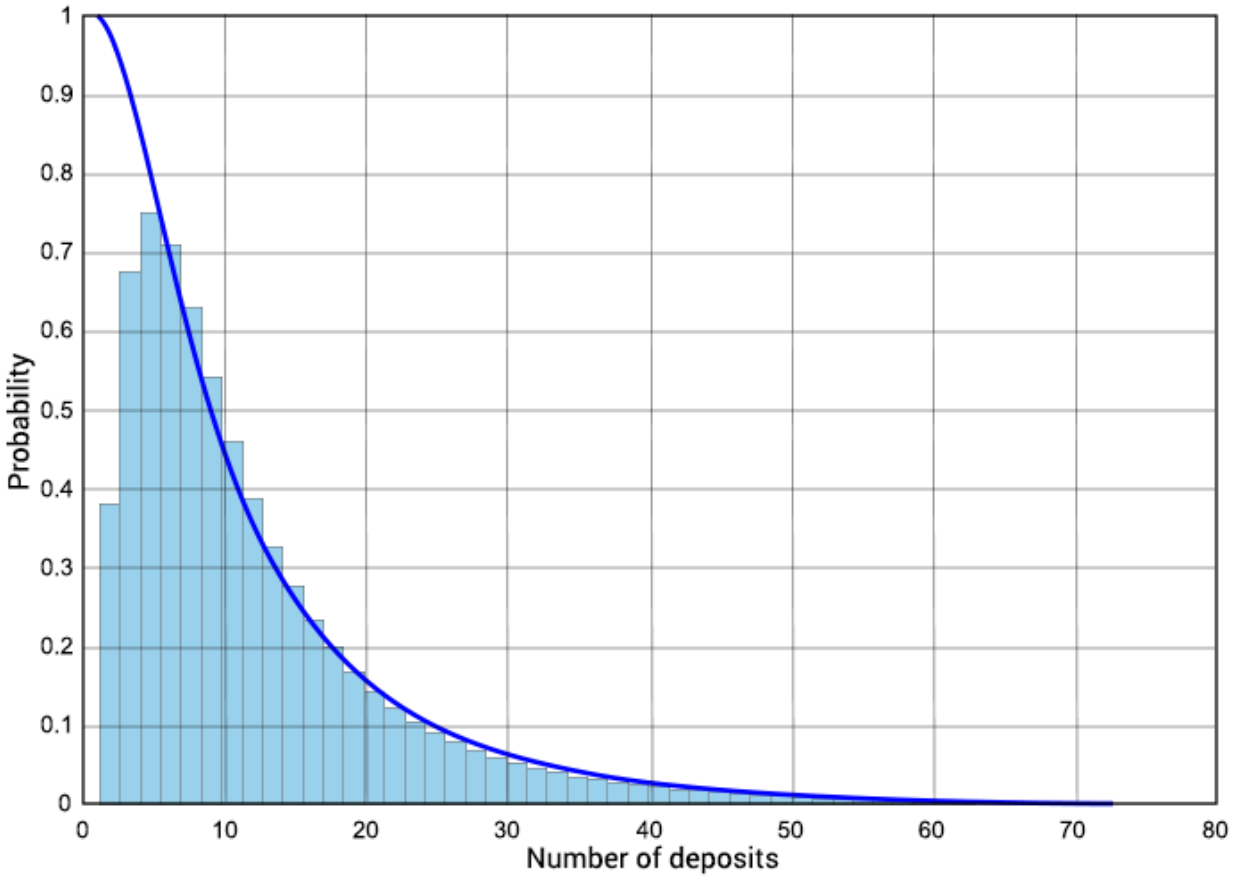

Fig. 6. Probability plot of the numbers of undiscovered deposits at neo-volcanic zones along the Mohn's Ridge.